Available online at www.sciencedirect.com
ScienceDirect
Ceramics International 37 (2011) 3703–3715
CERAMICS INTERNATIONAL
www.elsevier.com/locate/ceramint

Effects of manganese doping on properties of sol–gel derived biphasic calcium phosphate ceramics

I. Sopyan [a,*], S. Ramesh [b], N.A. Nawawi [a], A. Tampieri [c], S. Sprio [c]

[a] Department of Manufacturing and Materials Engineering, Faculty of Engineering, International Islamic University Malaysia (IIUM), PO Box 10, 50728 Kuala Lumpur, Malaysia
[b] Centre of Advanced Manufacturing and Materials Processing (AMMP), Department of Manufacture and Engineering Design, Faculty of Engineering, University of Malaya, 50603 Kuala Lumpur, Malaysia
[c] Institute of Science and Technology for Ceramics (ISTEC), Via Granarolo 64, 48018 Faenza, Italy

Received 13 May 2011; received in revised form 31 May 2011; accepted 15 June 2011
Available online 23 June 2011

Abstract

We have investigated the effect of manganese (Mn) doping on properties of nanosized biphasic calcium phosphate powders and their dense bodies. Manganese levels of 0.6, 1.3, 1.9, 4.3, 7.0 and 11.9 at.% were successfully incorporated into biphasic calcium phosphate via a sol–gel route. The prepared powders were calcined at temperatures of 500–1200 °C. The X-ray diffraction analysis revealed that a mix phase comprising of hydroxyapatite and β-tricalcium phosphate were present, however the content of each phases in the structure was affected by the Mn content. The studies found that the largest portion of β-tricalcium phosphate was detected at 4.3 at.% Mn doping. The incorporation of Mn has also greatly increased the crystallinity of the biphasic calcium phosphate powder due to progressive densification of particles. Characterization on their sintered dense bodies showed that manganese concentration affected the physical properties of the dense bodies. The highest density was found for 4.3 at.% Mn doped biphasic calcium phosphate sintered at 1300 °C.

Keywords: Mechanical properties; Biphasic calcium phosphate; Manganese doping; Sol–gel; Physical properties; Dense bodies

1. Introduction

Hydroxyapatite (HA), $Ca_5(PO4)_3(OH)$, whose chemical composition close to the mineral phase of bone is well known for its excellent biocompatibility with bone tissue. Representing ca. 69 vol.% of human bone, the mineral component of bones consists of poorly crystalline, Ca-deficient HA substituted partially with sodium, magnesium, citrate, carbonate and fluoride ions [1]. Together with β-tricalcium phosphate (β-TCP), $Ca_3(PO4)_2$, HA has been for nearly three decades the most extensively used substitution materials for artificial bone grafts. Although many problems concerning infective risk, mechanical and biological stability, compatibility, storage and costs still remain, HA materials have been applied in orthopaedic as block implants, porous scaffolds, granules or coating materials [2].

Biphasic calcium phosphate (BCP) ceramics, a mixture of HA and β-TCP, on the other hand, have also received much attention in the field of biomaterials. These materials, regarded as suitable for synthetic bone applications, are considered superior when compared to either single phase HA or β-TCP components because of their unique dissolution characteristics which in turn promotes new bone formation at the implant site [3]. These two compounds have different resorbing capacities. β-TCP degrades about 20 times faster than HA, therefore for practical purposes, HA is considered as non-degradable while β-TCP is resorbable [4]. Although single phase HA is stable, it is not biodegradable and therefore the implant could not be replaced by hard tissues in the body. Moreover, its application is constrained to non-load bearing region in clinical orthopaedic and dental applications due to its brittleness and low fracture toughness [5]. In the case of β-TCP, it was found that its application as a biomaterial for alveolar ridge augmentation resulted in a very high rate of biodegradation [6] which makes it unfavourable too. In addition, a disadvantage of β-TCP as

* Corresponding author. Tel.: +60 361964592; fax: +60 361964477.
E-mail address: sopyan@iium.edu.my (I. Sopyan).

0272-8842/$36.00
doi:10.1016/j.ceramint.2011.06.033

an implant material is its much lower low mechanical strength than HA. Therefore, it is envisaged that a mixture of HA and β-TCP would be appropriate as these two materials qualities off set each other's weaknesses. With a combination of enhanced bioactivity and mechanical stability difficult to achieve in single phase materials, characterization of BCP is of great importance and its characterization has consequently been well studied recently [7].

The inclusion of trace metal elements has a significant role in improving the physical and/or chemical properties of bioceramics. Many trace metal elements have been incorporated into the HA phase. In this work, manganese (Mn) was incorporated into the BCP as a sintering additive to improve the mechanical properties of dense BCP. Although numerous works have reported the significant role of manganese oxide in promoting densification in other ceramics systems, the inclusion of Mn in BCP has not been studied extensively [5]. The doping process were carried out chemically via an adapted sol–gel technique rather than by a physical method as reported by other researchers such as wet milling [5], mixing in an agate mortar [8] and ball milling [9].

The effect of Mn as a dopant on the stability and particle growth of HA has been investigated by some researchers. This dopant has been doped into calcium phosphate based materials by solid state reaction [10] and precipitation methods [10,11]. The motivation for the addition of Mn^{2+} ions to HA was due to the fact that divalent Mn^{2+} influences the activation of integrins, a family of receptors that mediate cellular interactions with the extracellular matrix and cell surface ligands [10,12]. The ligand affinity increases in the presence of Mn, resulting in the promotion of cell adhesion. In one study, manganese in the bone was found to cause a decrease in bone resorption [13]. It is also reported that Mn functioned as calcination and sintering additives of BCP powders without producing other secondary phases like α-TCP and CaO [5]. The formation of the α-TCP phase during the sintering process is not preferred as it induces micro-cracks, which eventually reduce the mechanical properties of the sintered specimens.

The doping of Mn into BCP is expected to show improvements in physico-chemical properties of BCP which will lead to improved biological performance in terms of bioactivity and bone mineralization. In a preliminary report, we have briefly described the synthesis of manganese doped BCP powder via a sol–gel technique [14]. Sol–gel method has been for the first time applied to synthesize hydroxyapatite powder by Sakka and co-workers using metal alkoxides as the monomers [15]. In this work, calcium nitrate tetrahydrate, manganese nitrate tetrahydrate, and *di*-ammonium hydrogen phosphate were used as the reactants. The calcined sol–gel powders were then subjected to uniaxial pressing to obtain the dense Mn-BCP bodies and then sintered at various temperatures. We present here the interesting effects of Mn content on phase behaviour, physico-chemical properties and the microstructure of the biphasic calcium phosphate (BCP) powder as well as of their dense bodies.

2. Experimental procedure

2.1. Preparation of powder

Calcium nitrate tetrahydrate [$Ca(NO_3)_2{\cdot}4H_2O$], di-ammonium hydrogen phosphate [$(NH_4)_2HPO_4$] and manganese (II) nitrate tetrahydrate [$Mn(NO_3)_2{\cdot}4H_2O$] were used as starting chemical precursors. Ethylenedinitrilotetraacetic (EDTA) acid (Titriplex II) (Merck kGaA, Germany) was added to 250 mL ammonium solution (11% solution, R&M Chemicals, UK) heated to 60 °C while stirring until it dissolved. In this technique, EDTA was used as chelating agent to prevent immediate precipitation of calcium compounds in the course of gel formation. A 100 mL aqueous solution of 65 g Ca $(NO_3)_2{\cdot}4H_2O$ (Merck kGaA, Germany) was then poured into the mixture followed by the dopant, 50 mL $Mn(NO_3)_2{\cdot}4H_2O$ (Merck kGaA, Germany). The addition of the $Mn(NO_3)_2{\cdot}4H_2O$ was based on the desired percentage (at.%) of manganese with regard to calcium to be doped into the BCP. The phosphorus precursor, 20 g di-ammonium hydrogen phosphate [$(NH_4)_2HPO_4$] (Merck kGaA, Germany) and 22.6 g urea (R&M Chemicals, UK), which acts as gelling agent and ammonium donor agent were subsequently added. The mixture was then refluxed at 100 °C for 4–5 h while stirring until a white gel of the Mn-BCP mixture was obtained. The urea in the solution was homogenised with regard to concentration and pH by stirring. The nitrate ion removal, which involved the white gel phase passing through a transparent sol phase, was done in only one reactor. The transparent sol obtained was not transferred to another reactor for the gelling process to avoid any possibility of contamination while transferring. The gel obtained was then dried at 340 °C in ambient air and subsequently subjected to heat treatment under flowing air. The synthesis of Mn-BCP was carried out at six different molar concentrations of Mn that is 0.6 at.%, 1.3 at.%, 1.9 at.%, 4.3 at.%, 7.0 at.% and 11.9 at.%.

2.2. Preparation of dense samples

The pure BCP calcined powder and four Mn doped BCP powders with Mn levels of 0.6 at.%, 1.9 at.%, 4.3 at.% and 11.9 at.% were chosen to be directly compacted into disks with diameter 20 mm, at 200 MPa using Uniaxial Press (Carver, 4350L). The green bodies were then sintered in a furnace (Protherm, PLF 160/5) at temperatures ranging from 900–1400 °C at a heating rate of 2 °C/min and with a 2 h holding time.

2.3. Analytical characterization

The synthesized powder was calcined at 900 °C to reach the optimum crystalline phase and ensure complete removal of organic and inorganic substance. The calcinations were carried out in the furnace (Protherm, PLF 160/5) with a heating rate of 10 °C/min to achieve the predetermined temperature followed by a holding time of 3 h before being cooled to room temperature in the furnace. In addition, the 4.3 at.% Mn-BCP black gel was calcined at different temperatures ranging from

500 to 1200 °C to observe the effect of calcination temperatures on the phase changes of the BCP ceramics. Elemental analysis was performed to determine Mn level in the Mn doped BCP powder samples using a Perkin Elmer atomic absorption spectrometer (AAS), model AAnalyst 400. X-ray diffraction (XRD) studies on the calcined powders were carried out using the Shimadzu, XRD600 series diffractometer. Diffraction spectra were collected over the 2θ range of 20–50 °C using monochromated Cu Kα radiation (λ = 0.15406 Å) with a step size of 0.02°. The crystalline phases were determined from a comparison of the registered standard JCPDF (Joint Committee on Powder Diffraction File) database (HA: 09-0432, β-TCP: 09-0169) with the obtained powder diffraction files. The intensity ratio between HA and TCP in all synthesized powder was determined using the relative intensity ratio (RIR) method [4]. Lattice constants were determined by least square refinements from the well determined positions of the most intense reflections. The chosen reflection planes of (2 1 1), (1 1 2) and (3 0 0) for HA and (0 2 1 0), (2 1 4) and (2 2 0) for β-TCP were used for the calculation and the average value were listed The crystallite size in HA was evaluated according to the Scherer's formula via XRD and using the Nano-Sizer (Malvern, Nano-S). For chemical bonding analysis, the powders were directly placed onto the Attenuated Total Reflection (ATR) holder of a Fourier Transform Infrared Spectrometer (FTIR) (Perkin Elmer, Spectrum 100) and 16 scans were performed at a resolution of 2 cm^{-1} in order to follow the chemical evolution from the gel to the BCP. The measurements were carried out in transmission mode in the mid-infrared range (380–4000 cm^{-1}) at the resolution of 4 cm^{-1}. Surface morphology of the powder was evaluated using the Field Emission Scanning Electron Microscope (FESEM) (JEOL, JFM 6700F). Prior to imaging, the BCP powders were subjected to sputter coating (JEOL, JFC-1600) with a thin layer of platinum to improve their conductivity. Observation of the nanosized BCP powder at a higher resolution was performed using Transmission Electron Microscope (TEM) (JEOL, JEM-2010). Thermogravimetric analysis (TGA) was performed on the black gel of the synthesized powders in ambient air using the Perkin Elmer apparatus (Pyris Diamond TG/DTA) with 2 °C/min heating rate.

The phase analysis of the sintered dense samples was carried out by X-ray diffraction as described for the powder. The density of the dense samples was measured by water immersion technique (Alfa Mirage, MD-300S) and the relative density was calculated by taking 3.156 g/cm^3 as the theoretical density of HA. The average value of relative density was taken out of 5 readings. The morphology of the dense samples was also examined using Field Emission Scanning Electron Microscopy (FESEM) as described for the powder.

3. Results and discussion

3.1. Characteristics of the Mn-BCP powders

Fig. 1 shows UV–vis absorption bands of undoped and Mn-doped BCP powders calcined at 900 °C. An increase in Mn content has increased the color intensity of BCP powders to darker shades, as verified by the increased light absorption for higher Mn content. The intensity of the colour indeed increased with increasing Mn content and calcination temperature. For example, 0.6 at.% Mn-BCP bluish white remained the same at 800–1000 °C and eventually changed to blue at 1200 °C and finally as dark blue at 1400 °C. From a chemical perspective, the origin of the apatite blue colour was due to the presence of Mn^{5+} or MnO_4^{3-} ions at the PO_4^{3-} sites in the apatite crystal structure [5,16]. Besides that sintering at high temperature increases the level of oxidation (Mn^{2+} to Mn^{5+}) in the oxidizing atmosphere and also provides enough energy for the oxidized manganese ion to migrate within the crystal lattice [17].

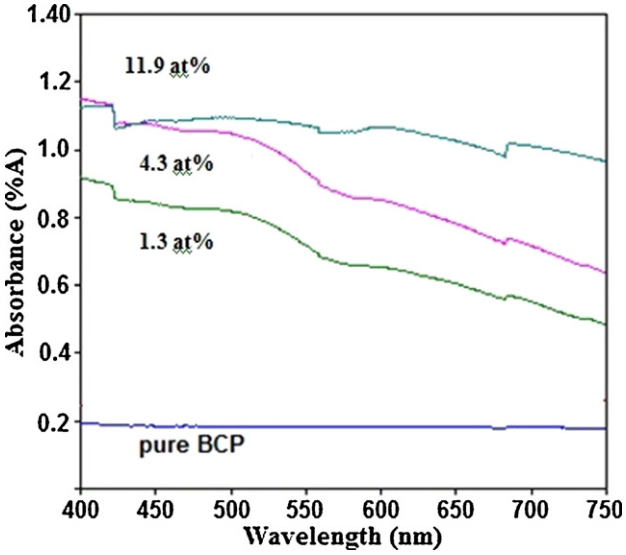

Fig. 1. UV–vis spectra of pure and Mn-doped BCP powders sintered at 1300 °C.

Fig. 2 presents the X-ray analysis of various Mn-BCP powders calcined at 900 °C. The calcination provided no crystalline phases other than HA as the main phase together with β-TCP as the minor phase. The diffraction patterns showed exclusively sharp clear reflections which confirmed the phase purity and high degree of crystallinity of the powder produced. All the detected peaks complied with the International Centre for Diffraction Data (ICDD) powder diffraction file #09-432 for HA and #09-0169 for β-TCP [9,14]. The presence of β-TCP phase is crucial as it verifies the formation of biphasic mixtures in the powder.

It was observed that doping of Mn greatly increased the crystallinity of the BCP powder even at only 0.6 at.% Mn level doped. An increase in the intensity of the β-TCP peak was compensated by an associated decrease in HA intensity and *vice versa*. Hence, it can be deduced that the formation of the β-TCP phase has suppressed the formation of the HA phase. The lack of TCP in the 0.6 and 1.3 at.% Mn-doped BCP powders could be attributed to the correct stoichiometric ratio of Ca:P during the synthesis [18]. It can be also seen that β-TCP peak intensity increased with the increasing Mn level doped, with the highest intensity of β-TCP peak at 4.3 at.% Mn. This powder, with the largest amount of β-TCP in the biphasic mixtures,

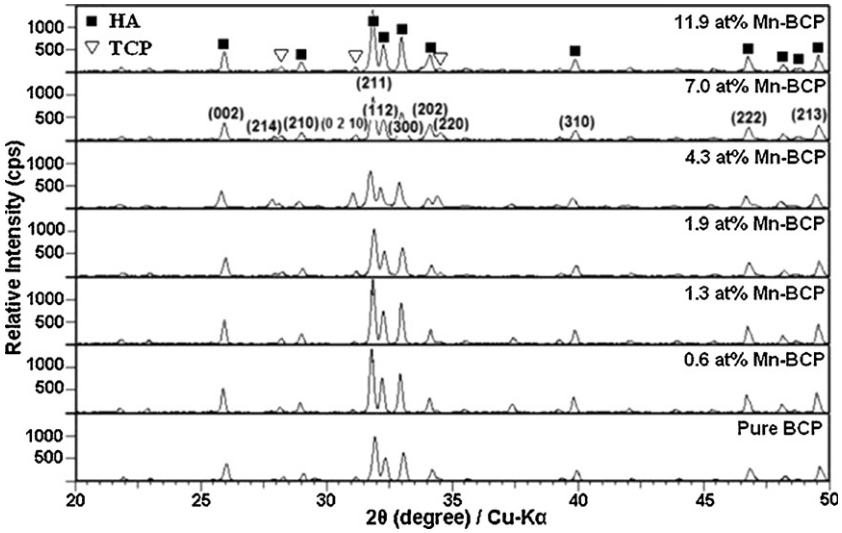

Fig. 2. XRD patterns of various Mn-BCP powders calcined at 900 °C. The symbols ■ and ▽ are assigned for HA and β-TCP phases, respectively.

might possess the highest Ca deficiency among all [17]. Moreover, the increase in β-TCP peak intensity with Mn content can be correlated with replacement of Ca ions by Mn ions [8–10,19]. This preference was supported by ionic size considerations, as Mn ion (0.83 Å) is smaller than Ca ion (0.99 Å) [9,18].

The 4.3 at.% Mn-doped BCP powder showed a shift in the β-TCP peaks to smaller 2θ angles. However, the HA peaks did not show any changes in their 2θ angles positions. This also supported the findings that Mn substitution favours TCP phase rather than HA phase, due to the solubility limit of Mn in HA. β-TCP contains a cation site of octahedral coordination which is smaller than cation site of HA, which is more suitable for the smaller Mn^{2+} than Ca^{2+} [18]. It can be inferred that doping of Mn < 4.3 at.% generated the formation of β-TCP as the secondary phase but beyond the concentration the solubility limit of the Mn in the β-TCP phase decreased, thus hindering the secondary phase formation.

The relative intensity ratio (RIR) of HA to TCP was determined using the intensities of the (2 1 1) and (2 0 1 0) peaks of the HA and β-TCP respectively using the formula, $RIR = I_{\beta\text{-TCP}}/(I_{\beta\text{-TCP}} + I_{HA})$ and the calculated ratio is presented in Table 1. The intensity quantitative values obtained are in good agreement with the observation found in Fig. 2 where the HA intensity increased with Mn content and β-TCP peak appearance has been at its most intense at 4.3 at.% Mn-doped BCP. The indefinite appearance of β-TCP peak for 0.6 and 1.3 at.% of Mn powders could be correlated to nearly 100% presence of HA in the powder themselves, that are 96% and 97%, respectively.

Differences in the calculated lattice parameters were observed for the BCP powders. The calculated lattice parameters of the HA peak presented in Table 2 revealed that the hexagonal structure characteristic of HA was retained in spite of the presence of Mn. However, there were apparent contractions in the cell parameters *a* and *c*. A slight but continuous decrease in *a* and *c* with increasing Mn content was observed.

It was previously stated that Mn-doped BCP samples crystallize in the *R*3*c* rhombohedral structure which is characteristic of β-TCP [9]. This is quantitatively supported by its calculated lattice parameters in Table 3 showing that both lattice parameters *a* and *c* decreased with the increasing Mn level doped. The significant contraction of the Mn-doped BCP

Table 1
Relative intensity ratio of HA and TCP in the powders.

Mn-BCP powder (at.%)	HA:TCP
0.0 (pure BCP)	93:7
0.6	96:4
1.3	97:3
1.9	90:10
4.3	72:28
7.0	89:11
11.9	94:6

Table 2
Calculated lattice parameters for HA in Mn-BCP powders calcined at 900 °C.[a]

Mn content (at.%)	*a*	*c*	*c*/*a*
0.0 (pure BCP)	9.397	6.861	0.730
1.9	9.394	6.850	0.729
7.0	9.384	6.844	0.729
11.9	9.408	6.873	0.730

[a] HAP-JCPDS PDF 09-432; *a* = 9.418 Å, *c* = 6.884 Å.

Table 3
Calculated lattice parameters for TCP in Mn-BCP powders calcined at 900 °C.[a]

Mn content (at.%)	*a*	*c*	*c*/*a*
0.0 (pure BCP)	10.342	37.581	3.633
1.9	10.320	37.539	3.634
7.0	10.314	37.517	3.637
11.9	10.325	37.591	3.641

[a] TCP-JCPDS PDF 9-0169; *a* = 10.429 Å, *c* = 37.38 Å.

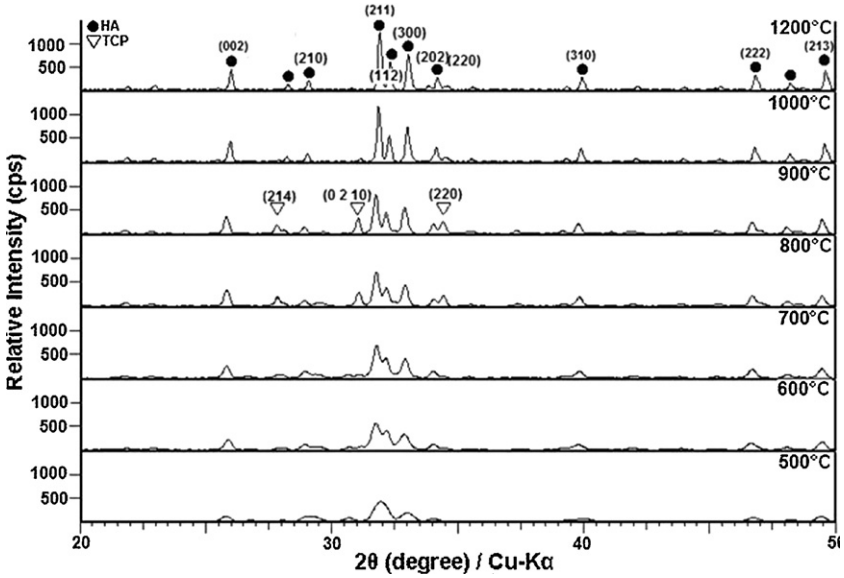

Fig. 3. XRD pattern of pure BCP calcined from 500 °C to 1200 °C. The symbols ● and ▽ are assigned for HA and β-TCP phases, respectively.

compared to the pure BCP may reflect the substitution of Ca^{2+} ion by smaller ionic radius of Mn^{2+} in the β-TCP phase [9]. The contraction of β-TCP lattice parameters with the increasing Mn doped is significantly greater than that of HA, showing Ca substitution by Mn in the β-TCP phase.

Investigation on the effect of calcination temperature (in the range of 500–1200 °C) on phase behaviour was conducted on pure BCP and 4.3 at.% Mn-doped BCP powder, and the measurements are presented in Figs. 3 and 4, respectively. XRD diffraction pattern for both samples at 500 °C showed a poorly crystalline apatite. The transformation from the amorphous phase to crystalline phase occurs in the range of 600–700 °C and 500–600 °C for pure BCP and 4.3 at.% Mn-doped BCP powders, respectively. The appearance of β-TCP started to be detected at 700 °C for 4.3 at.% of Mn and at 800 °C for pure BCP. The appearance of β-TCP peak is the evident of the transformation of deficient apatite to biphasic mixtures of HA and β-TCP. A similar study was also done on 0.6 at.% Mn-doped BCP and a transition to crystalline phase only occurred between 700 and 800 °C. At 900 °C, all the synthesized powders have showed the existence of β-TCP phase at highest resolution of peaks that confirmed the formation of biphasic mixtures at the optimum temperature. However, when the calcination temperature was increased up to 1200 °C, the XRD pattern of the powder has showed an increase in peak intensity of HA phases, accompanied by a reduction in β-TCP phase intensity. This result suggests that at higher calcination temperatures, reversible transformation of β-TCP phase into HA phase has occurred. Reversible transformation occurred via the replacement of dopant ion, in which free Ca expelled from TCP by Mn substitution in turn reacts with the β-TCP phase to form HA phase [18]. This is also in agreement with the decrease in the intensity of β-TCP as temperature increased from 900 to 1200 °C.

The FTIR spectra of various Mn-BCP powders calcined at 900 °C are displayed in Fig. 5. Calcined powders' spectra show vibrational bands characteristics of calcium phosphate compounds. The fundamental vibration modes of PO_4^{3-} group were

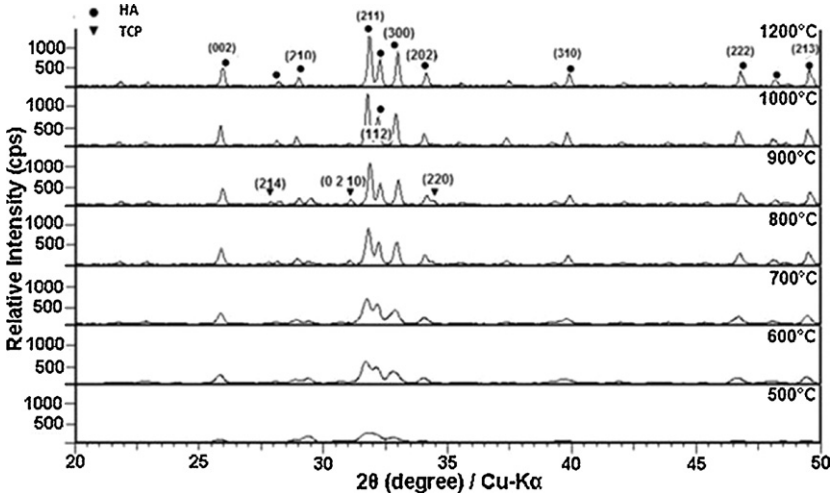

Fig. 4. XRD pattern of 4.3 at.% Mn-BCP calcined from 500 °C to 1200 °C. The symbols ● and ▼ are assigned for HA and β-TCP phases, respectively.

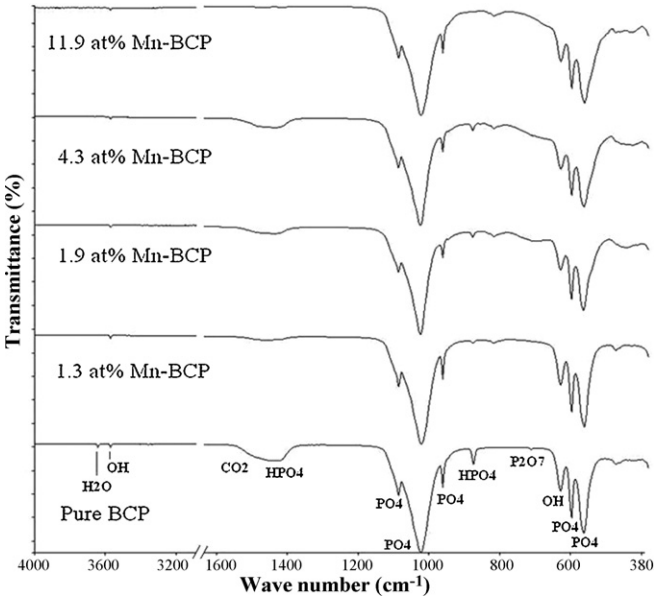

Fig. 5. FTIR spectra of Pure BCP and Mn-BCP powder at various Mn contents calcined at 900 °C.

spotted at 574 cm^{-1} (mode υ_4), 609 cm^{-1} (mode υ_4), 966 cm^{-1} (mode υ_1), 1024 cm^{-1} (mode υ_3) and 1086 cm^{-1} (mode υ_3) [17,20]. Among these bands, the strong band at 1086 cm^{-1} is attributed to a tri-calcium-phosphate (TCP) [21]. Meanwhile, the bands observed at 3570 and 630 cm^{-1} could be attributed to the presence of the hydroxyl (OH^-) group in a HA environment [17,21]. The band of OH^- increased in its intensity with Mn content. This is parallel with the XRD analysis showing the increase in HA crystallinity with Mn content. Nevertheless, the presence of the water band at 3600 cm^{-1} was detected in 1.3 at.% Mn-BCP sample and pure BCP only. All the BCP powders are also characterized by a broad band at 1380–1550 cm^{-1} which indicates the presence of carbonate (CO_3) groups. However, as the amount of Mn increased, the decrease in the intensity of the corresponding peaks has clearly pronounced the gradual loss of CO_3 bands from the FTIR spectra [17].

Referring to the XRD pattern of 4.3 at.% Mn-BCP in Fig. 2, it can be seen that the powder contains the largest amount of TCP among all the powders. This is confirmed by its FTIR spectra where the OH^- band at 630 cm^{-1}, which belongs to HA phase, has less intensity than those of 1.9 and 11.9 at.% powders.

The presence of HPO_4^{2-} detected at 875 cm^{-1} in the FTIR spectra for Mn-doped BCP powders shows that these powders behaves similarly to calcium deficient apatites without any substituted elements [17]. It was observed that the decrease in HPO_4^{2-} band intensity is compensated by the appearance of $P_2O_7^{4-}$ band (715 cm^{-1}). With the increasing Mn content, the decrease in HPO_4^{2-} band became intense accompanied by the increase in $P_2O_7^{4-}$ band's intensity. This phenomenon is verified as the condensation of HPO_4^{2-} to yield $P_2O_7^{4-}$ [20,22]. It is reasonable to deduce that the anion of HPO_4^{2-} exists in less crystalline phase and its condensation is completed as some amount of dopant were added into BCP.

The TGA plots of pure and Mn-BCP black gels are shown in Fig. 6. From room temperature to about 250 °C, incorporated water is lost [23]. A continuous weight loss was observed between 250 °C and 550 °C, which can be associated with the burning of organic substances and by-products such as NO_3^- and ammonia which become volatile upon heating. These by-products are absorbed on the surface only as there is no study reported on NO_3^- incorporation into the apatite structure and while the incorporation of ammonia ions is very limited due to their large size [21]. The weight loss also was described as the oxidation of the residual solvents and vigorous decomposition of the organic and inorganic precursors at 440 °C [24]. It is also reported that at approximately 400 °C, the condensation reaction of hydrogen phosphate ions has took place [25]. This reaction facilitates the formation of TCP upon heating with the increasing Mn concentration. This judgement is in good agreement with this research study. Furthermore, in that temperature range, all samples showed similar weight loss of about 50% indicating that the calcination has changed the amorphous phase of the black gel to the crystalline phase of BCP.

The steps of weight loss between 700 and 800 °C show the characteristics of calcium deficient apatite. From 710 °C up to

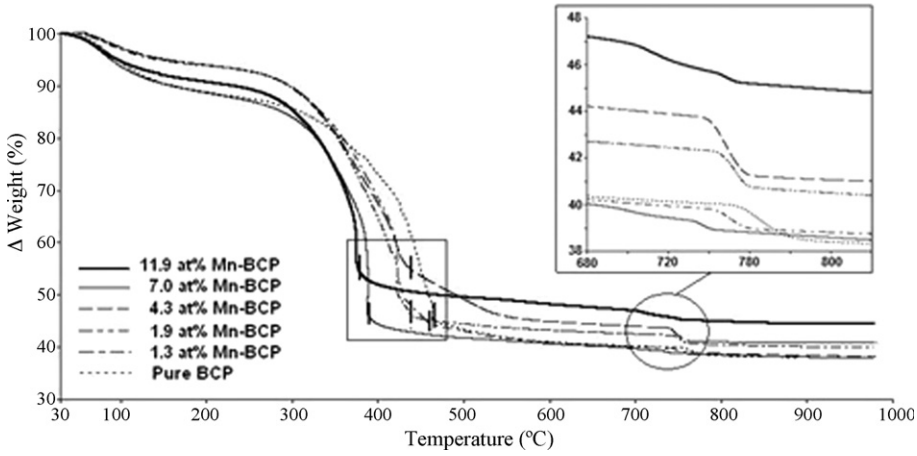

Fig. 6. TGA curve of Mn-BCP black gels analyzed up to 900 °C. The square and circle marks are assigned for the formation of HA and β-TCP, respectively.

Table 4
HA crystallization and TCP formation temperatures at various Mn contents.

Mn content (at.%)	Start of HA crystallization temperature (°C)	TCP formation temperature (°C)
0.0 (pure BCP)	465	754
1.3	453	743
1.9	439	740
4.3	433	735
7.0	394	714
11.9	380	704

800 °C, the decomposition of HPO_4^{2-} and $P_2O_7^{4-}$ to biphasic mixtures was detected, accompanied by the weight loss of about 2% of all the samples [22]. This was derived from the condensation of the HPO_4^{2-} groups to yield calcium pyrophospate, $Ca_2P_2O_7$, which at higher temperatures, react further with HA to yield $Ca_3(PO_4)_2$ [20,22].

The TGA plot also revealed that as Mn content increases, the crystallization and decomposition to biphasic mixtures occurred at a lower temperature. Table 4 lists the starting temperature for crystallization of HA and the decomposition temperature of pyrophosphate to biphasic mixtures. The result reveals that doping of Mn up to 11.9 at.% has reduced the crystallization temperature of HA and formation temperature of biphasic mixtures. From the 11.9 at.% Mn-doped BCP plot, it can be seen that HA crystallization and TCP formation occurred at the temperature of about 381 °C and 704 °C, respectively. In fact, the 11.9 at.% Mn-doped BCP shows the lowest temperatures for both the HA crystallization and the TCP formation among all the Mn-doped BCP samples. In addition, the 4.3 at.% Mn-BCP black gel experienced the sharpest weight drop at 750 °C as it decomposed to biphasic mixtures. This was supported by XRD analysis (Fig. 2) and calculated ratio of HA/β-TCP (Table 1), where highest intensity of β-TCP phase is portrayed by 4.3 at.% Mn-doped BCP.

Fig. 7 shows a TEM image of pure BCP powder (a) and FESEM images of the Mn-BCP powders at different Mn molar percents (b–d). The TEM revealed nanometric primary particles with individual size distribution between 10 and 20 nm are globular in shape, but tightly agglomerated into submicro- and microscale aggregates. FESEM measurement revealed that doping of Mn into BCP particles caused fusion of particles leading to larger individual particles. The lower intensity and peak broadening of the diffraction pattern of this powder compared to the doped powders shown in Fig. 2 is in agreement with this observation. FESEM showed that doping of Mn into BCP particles caused fusion of particles leading to more progressive densification of particles as shown by 11.9 at.% Mn doping. As Mn increased to 11.9 at.%, Mn-doped BCP powders showed no longer spherical shape but flat-

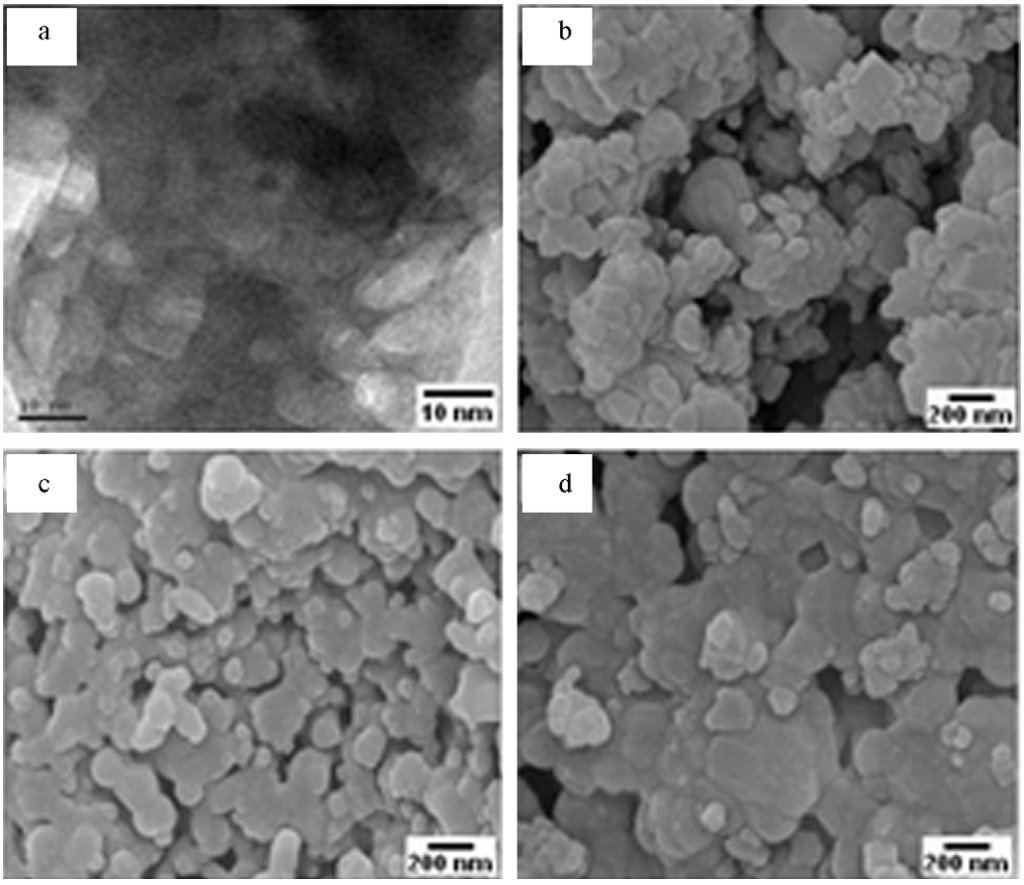

Fig. 7. (a) TEM picture of Mn-BCP powder and FESEM images of Mn-BCP powders of (b) 4.3 at.% Mn, (c) 7.0 at.% Mn and (d) 11.9 at.% Mn doping.

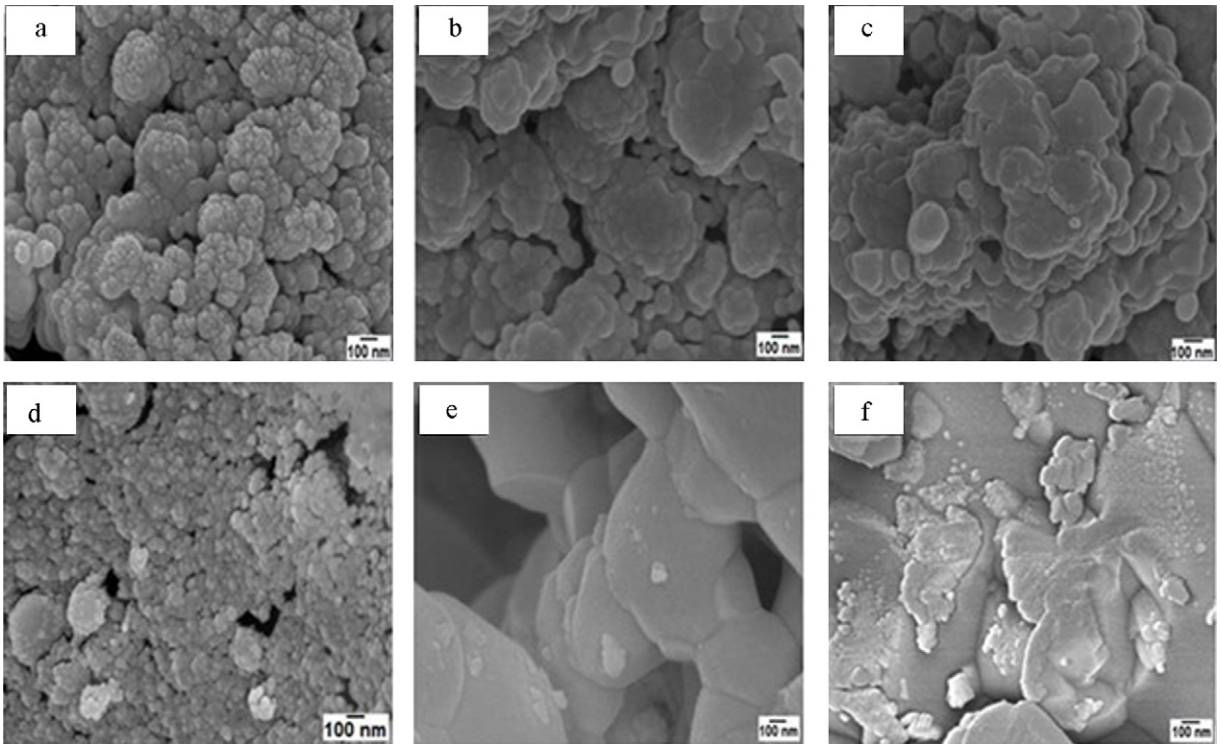

Fig. 8. SEM images of pure BCP powers calcined at 500 °C (a), 1000 °C (b) and 1200 °C (c) and of 4.3 at.% Mn doped BCP powders calcined also at 500 °C (d), 1000 °C (e) and 1200 °C (f).

like structure as the particles are well grown and densified. This fusion of particles has started to be observed at the doping of 4.3 at.% where the globular shapes have begun to flatten. At 7.0 at.% of Mn, the aggregates are still likely in globular shapes but micrometric aggregates are getting bigger as the spherical particles melted and densified due to the fusion of the particles. Earlier fusion of particles was similarly observed for Mn doped BCP powders in respect of pure BCP when calcined at higher temperatures. Fig. 8 shows pure BCP powders calcined at 500 (a), 1000 (b) and 1200 °C (c) and 4.3 at.% Mn doped BCP powders also calcined at 500 (d), 1000 (e) and 1200 °C (f). The change in the microstructures of the powders could be observed in terms of the increase in size of the agglomerated globular particles with increased calcination temperatures. For the lowest calcination temperature, 500 °C, the morphology of the pure BCP powders appeared to be composed of fine individual crystallites in nano size (∼12 nm in average as measured by Scherer's equation), spherical shapes and tightly agglomerated. The particles enlarged to 55 nm and 59 nm after the calcinations of 1000 °C and 1200 °C, respectively.

For the 4.3 at.% Mn-doped BCP powder, initially the nano size crystallites are spherical in shape with the size of 16 nm. At 1000 °C calcination temperature, the individual particles tend to melt together as more progressive densification of particles occurred at this temperature and the particle has enlarged to 61 nm. The fusion of particles can be seen clearly when the 4.3 at.% Mn-doped BCP powder was calcined at 1200 °C (65 nm) where the crystallites are no longer in their spherical shape but totally densified forming flat surface. From the figure, we can conclude that increasing the calcination temperature has increased the coarsening of the microstructure of the powder particles whereby the spherical crystals are well growth as they melt and diffuse together. This is in good agreement with the XRD analysis which indicates increasing crystallinity of the 4.3 at.% Mn-BCP with larger crystallite size.

Fig. 9 shows FTIR spectra of (a) pure BCP and (b) 4.3 at.% Mn-doped BCP powders respectively calcined at different temperatures ranging from 500–900 °C. Both spectra showed that C–O band at 1300–1600 cm^{-1} decreased in its resolution increasing calcination temperature. The decrease in carbonate band has simultaneously increased the OH^- and PO_4^{3-} bands. This finding shows that the formation of the BCP phase involved a substitution of carbonate groups for hydroxyl (A-type) and the phosphate (B-type) groups. It was also observed that the presence of PO_4^{3-} band (1086 cm^{-1}) which belongs to the TCP phase has been detected in between the temperature of 700–800 °C. This result is in good agreement with the result of TG analysis in Fig. 6. The spectrum revealed the presence of hydrogen phosphate groups (HPO_4^{2-}) and pyrophosphate ($P_2O_7^{4-}$) bands are evident at 500 °C by the peak at 875 cm^{-1} and 715 cm^{-1}, respectively. However, as the temperature increases, these two bands are viewed with a decreasing intensity, leading to a conclusion that this anion, HPO_4^{2-} exist in less crystalline phase. This confirms the formation of biphasic mixtures of HA and that Mn has stabilized β-TCP in the synthesized powder when calcined at higher temperatures. Nevertheless, profound change in OH^- band intensity at 630 cm^{-1} was observed as the temperature increases from 700 to 900 °C. This can be attributed to the increase in HA crystallinity with the increasing calcination temperatures [23]

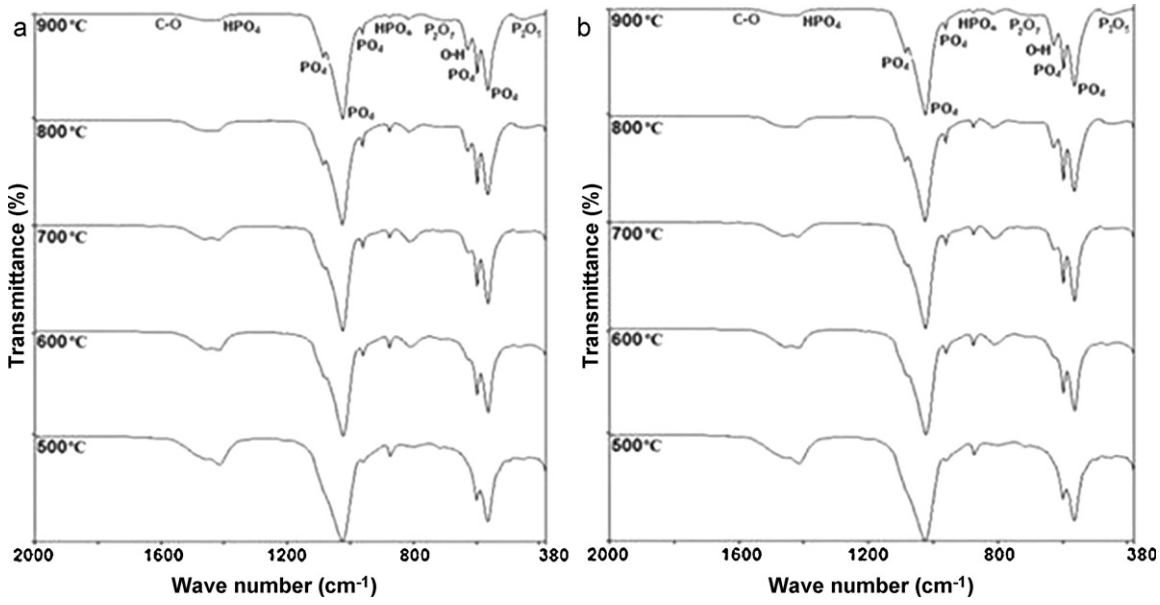

Fig. 9. FTIR spectra of pure BCP (a) and 4.3 at.% Mn-doped BCP (b) powders calcined at 500–900 °C.

as also supported by XRD patterns in Figs. 3 and 4. It is clear, particularly from Fig. 9(b), that HPO_4^{2-} band's intensity decreases with the increasing calcinations temperature, indicating disappearance of $CaHPO_4$ due to condensation to calcium pyrophosphate.

3.2. Characteristics of the Mn-BCP dense samples

The dense samples of Mn-BCP appeared in different color shades according to Mn content and sintering temperature as observed in their powder state; higher Mn content or higher sintering temperature results in darker gray shades. Fig. 10 shows the XRD pattern of various concentrations of Mn-BCP dense samples sintered at 1300 °C. The results show the present of a HA single phase when compared to the XRD traces of the powders (Fig. 2) which had both, the HA and β-TCP phases. Apparently, a phase conversion during the sintering of the dense biphasic mixture has occurred, converting all β-TCP into HA.

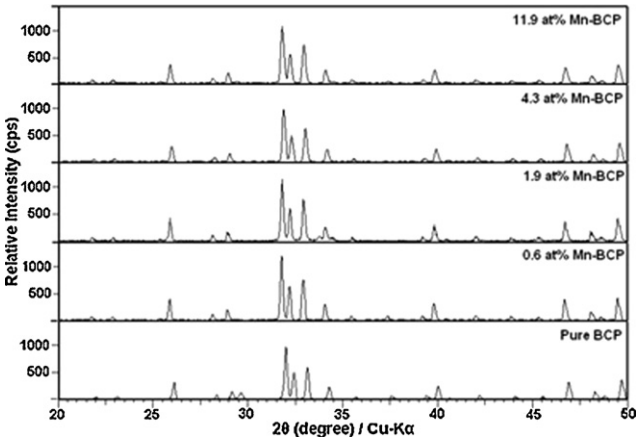

Fig. 10. The XRD patterns of the Mn-BCP dense bodies after sintering at 1300 °C.

The phase conversion took place at all sintering temperatures of 900–1400 °C. It has been suggested by Kong et al. that this newly formed apatite plays some crucial role in the biocompatibility of the biphasic ceramics [26]. Another observation was that no decomposition of biphasic mixtures to secondary phases such as CaO and α-TCP takes place even when it is consolidated at high temperatures above 1200 °C.

Generally, the density variation of all the studied compositions exhibited a similar trend with increasing sintering temperature. The measurements are summarized in Table 5. The undoped BCP could only achieve the highest value of 91% at 1300 °C, which could be achieved by 4.3 at.% Mn-doped BCP at a lower temperature of 1200 °C. However, it still shows a notable increase in density with increasing temperature. For 0.6 at.% Mn and 1.9 at.% Mn, the maximum densification of 92% and 93%, respectively, was attained at 1300 °C. Meanwhile, 11.9 at.% Mn only attained the highest of 98% relative density when sintered at 1400 °C as compared to 4.3 at.% Mn which attained 99% densification at 1300 and 1400 °C. It was found that sintering above 1300 °C was required to achieve 98% of theoretical density [27]. This difference in finding could be related to the difference in powder characteristics used. If sintering was carried out above the onset of densification temperature, it would result in only small increment of density due to the final stage of sintering whereby small levels of porosity are removed and the grain growth begin [28].

It was observed that an increase in Mn content and sintering temperature has improved the densification behaviour of the BCP. It can be seen from Table 5 that sintering at 1000 °C, for example, has resulted in massive improvement of densification for Mn doped BCP. The relative density has increased from 86% to 88% with only 1.9 at.% of Mn doped into the BCP. The further increase to 89% and 90% were found for 4.3 at.% and 11.9 at.% of Mn doping, respectively. At 1300 °C sintering temperature, the densification was pronouncedly increased to 99% for

Table 5
Average relative density of pure BCP and Mn-BCP dense samples at various sintering temperatures.

Sintering temperature (°C)	Dense samples				
	Pure BCP	0.6 at.% Mn	1.9 at.% Mn	4.3 at.% Mn	11.9 at.% Mn
800	80 ± 0.04	82 ± 0.02	85 ± 0.03	87 ± 0.02	89 ± 0.02
900	82 ± 0.02	83 ± 0.03	86 ± 0.02	88 ± 0.05	89 ± 0.01
1000	86 ± 0.01	86 ± 0.04	88 ± 0.03	89 ± 0.01	90 ± 0.01
1100	87 ± 0.02	88 ± 0.03	89 ± 0.02	91 ± 0.02	90 ± 0.03
1200	90 ± 0.02	90 ± 0.02	91 ± 0.02	92 ± 0.02	93 ± 0.03
1300	91 ± 0.02	92 ± 0.02	93 ± 0.02	99 ± 0.20	96 ± 0.20
1400	90 ± 0.01	91 ± 0.03	92 ± 0.05	99 ± 0.20	98 ± 0.03

4.3 at.% Mn compared to 91% and 92 of relative density for pure and 1.9 at.% Mn-doped BCP. While doping of 0.6 and 1.9 at.% Mn only gave moderate improvement in density for all sintering temperatures, 4.3 at.% Mn doping shows significant density improvement particularly for 1300 and 1400 °C sintering. In this study, 4.3 at.% Mn-doped BCP exhibited the highest densification of 99% at 1300 °C among all the samples. It is believed that β-TCP phase present in the 4.3 at.% Mn starting powder play important role in densification during sintering. This more progressive densification is presumably due to higher thermal stability of BCP phase as thermal stability of the starting powder allowed the samples attaining fully densification at high sintering temperature [29]. It was reported that the sintered HA samples achieved a maximum of 76.8% and 82.4% of theoretical density at 1200 °C and 1340 °C, respectively [28]. The 4.3 at.% Mn-doped BCP has lower HA crystallinity and resulted in smallest particle size (40 nm) compared to the other powders (which are in the range of 44–59 nm). This feature may contributed to the 4.3 at.% Mn sample's most progressive densification [30]. Some investigators also reported that this was probably due to the higher surface area which promoted a large driving force for densification [31,32].

The microstructural evolution of the pure BCP and Mn-doped BCP dense ceramics sintered at 1000–1400 °C were

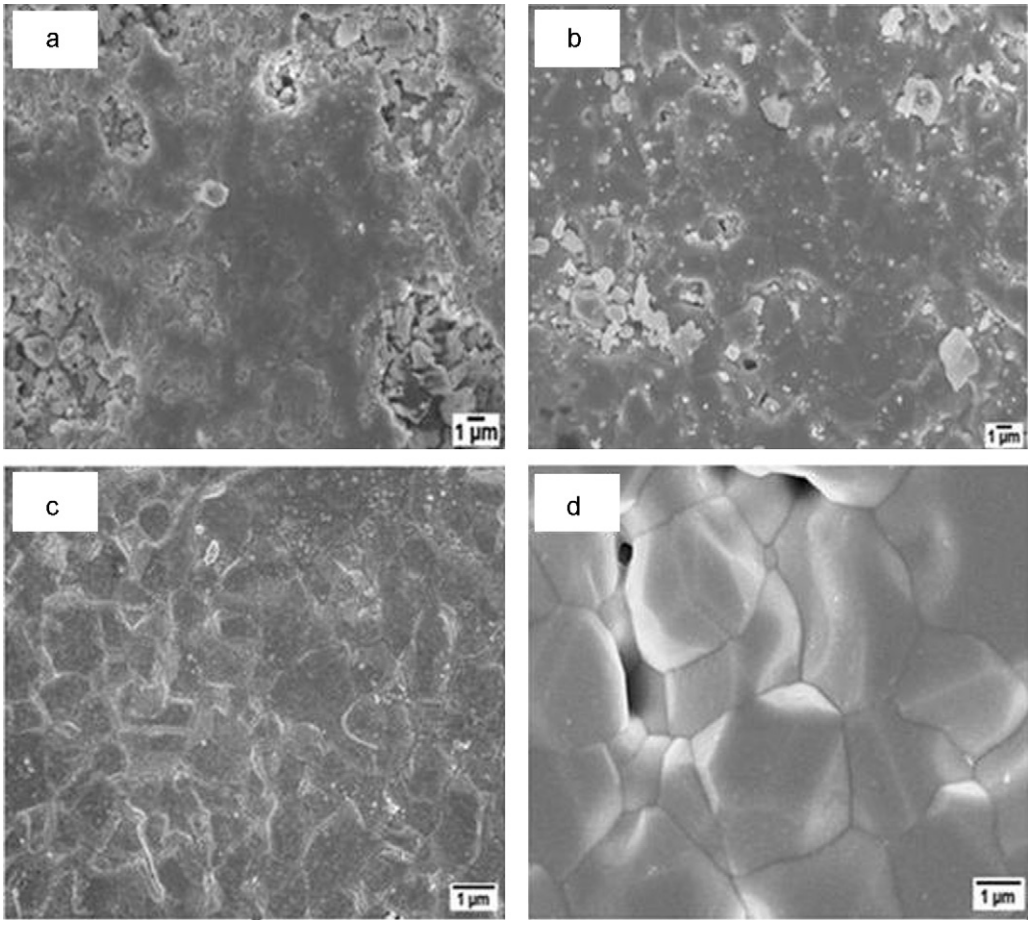

Fig. 11. SEM images of (a) pure BCP, (b) 0.6 at.% Mn-doped BCP, (c) 4.3 at.% Mn-doped BCP, and (d) 11.9 at.% Mn-doped BCP dense samples sintered at 1300 °C.

carried out to determine the microstructure and grain size. It was observed that sintering at 1000 °C exhibited an almost dense microstructure for 11.9 at.% Mn-doped BCP which corresponds to a relative density of 90% with grain size in the range of 0.157–0.73 μm. However, porosity is still visible at some part due to the occurrence of only first stage sintering. In terms of Mn content, it was found that at this particular temperature, pure BCP and 0.6 at.% samples showed remnant of porosity in the microstructure which also correspond to the only first stage sintering or incomplete densification of structure during the sintering process which resulted in mere formation of solid bridges between grains [33]. For 1.9 at.% Mn, it was observed that the densification has started to take place where the microscale aggregates has started to formed dense surface as the spherical particles melted and densified due to more progressive fusion of the particles.

As the temperature was increased to 1300 °C, the densification accelerated as the amount of pores has been greatly reduced for the pure BCP powder as shown in Fig. 11(a). All the Mn-doped BCP showed a denser microstructure. For 0.6 at.% Mn, the residual porosity observed at 1000 °C was removed with the relative density of 92%. At 1.9 at.% Mn, the densification became more progressive as it can be seen the grain boundary become visible, which indicates that the presence of Mn as sintering additive also contribute to the improvement of grain boundary properties of BCP [34]. As the Mn content increased to 4.3 at.%, denser microstructure with 99% of theoretical density and no residual porosity was observed as Fig. 11(c) shows. 11.9 at.% Mn sample exhibited significant grain growth, with individual grains reaching up to 3–6 μm in size as shown in Fig. 11(d).

Fig. 12 shows the effect of Mn content at various sintering temperatures on the BCP samples. This investigation, for comparison purpose, was emphasized on pure BCP and 4.3 at.% Mn-doped BCP samples. It was clear that the densification at 1000 °C was greater with doped BCP sample as the porosity has been reduced significantly at the onset densification temperature. At 1200 °C, the microstructures are denser for both the concentrations than the previous sintering temperature. At 1300 °C, the grain growth has become more

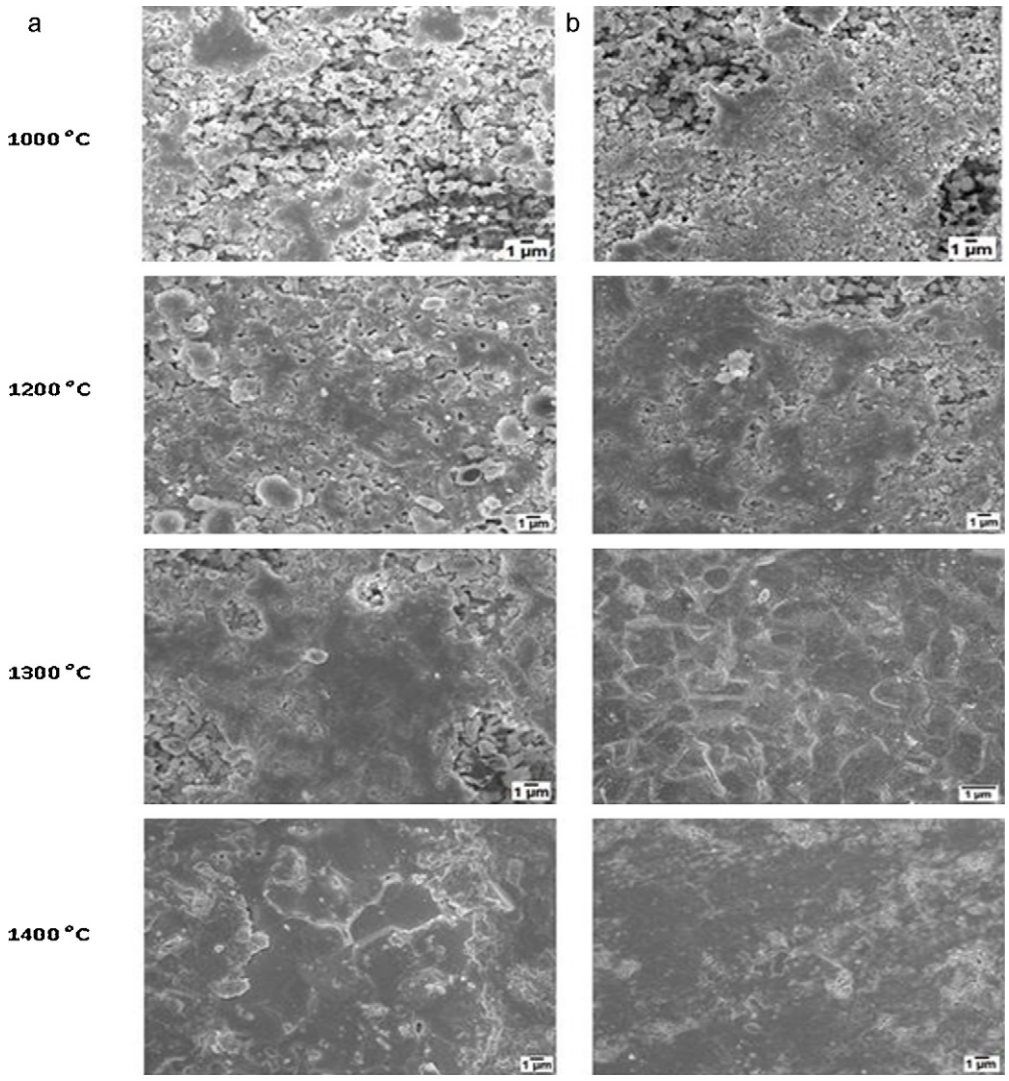

Fig. 12. SEM images of (a) pure BCP and (b) 4.3 at.% Mn-doped BCP sintered compacts at various sintering temperatures.

visible and progressive for 4.3 at.% compared to the undoped BCP which resulted in complete sintering due to the absence of porosity on the microstructure. For pure BCP, the grain growth has only started at 1400 °C while 4.3 at.% Mn-doped BCP has experienced complete densification at this temperature where the grain boundaries has started to melt and diffuse into the grain. It has been reported that grain growth was due to the improvement in the homogeneity of the powder with increasing sintering temperature, and it occurred especially when sintering was carried out from 1200 °C to 1400 °C [28,35].

4. Conclusions

Nanosized powders of manganese doped biphasic calcium phosphate and their dense bodies have been successfully prepared. The synthesized powders consist of only HA and β-TCP phases with slight changes in the lattice parameters after Mn doping. The Mn ion substituted Ca ion in the β-TCP phase rather than in the HA phase and has greatly enhanced the crystallinity of the BCP powder. Crystallinity of BCP powder increased with increasing Mn content and this was attributed to more progressive fusion and densification of the particles during sintering. The increasing Mn content has also lowered the crystallization temperatures of HA and accelerated TCP formation through the decomposition of HA. The amount of Mn added in the BCP powder was also found to affect the phase content of hydroxyapatite (HA) and β-tricalcium phosphate (β-TCP) in the sintered matrix. BCP with the largest portion of β-TCP was found at 4.3 at.% Mn doping which resulted in enhanced densification of the sintered body. In dense Mn-BCP bodies, the phase conversion of β-TCP to HA occurred during all sintering regimes leading to formation of HA phase only. This study showed that the presence of manganese improves the densification of the BCP mixture as the relative density increased with sintering temperature and Mn content. The maximum relative density was achieved at 99% by 4.3 at.% Mn-BCP sample sintered at 1300 °C. Mn has successfully functioned as a sintering additive for the sol–gel derived BCP powders.

Acknowledgements

The authors would like to acknowledge the financial support provided by Ministry of Science, Technology and Innovation (MOSTI) under the eScience Fund programme (Project No. 03-01-08-SF0020).

References

[1] H. Yuan, K. de Groot, Calcium phosphate biomaterials: an overview, NATO Sci. Ser. II 171 (2005) 37–57.
[2] I. Sopyan, M. Mel, S. Ramesh, K.A. Khalid, Porous hydroxyapatite for artificial bone applications, Sci. Technol. Adv. Mater. 8 (2007) 116–123.
[3] S. Kannan, J.M.G. Ventura, A.F. Lemos, A. Barba, J.M.F. Ferreira, Effect of sodium addition on the preparation of hydroxyapatite and biphasic ceramics, Ceram. Int. 34 (2008) 7–13.
[4] E.C. Victoria, F.D. Gnanam, Synthesis and characterisation of biphasic calcium phosphate, Trends Biomater. Artif. Organs 16 (2002) 12–14.
[5] S. Ramesh, C.Y. Tan, C.L. Peralta, W.D. Teng, The effect of manganese oxide on the sinterability of hydroxyapatite, Sci. Technol. Adv. Mater. 8 (2007) 257–263.
[6] N. Kivrak, A.C. Tas, Synthesis of calcium hydroxyapatite–tricalcium phosphate (HA–TCP) composite bioceramic powders and their sintering behavior, J. Am. Ceram. Soc. 81 (1998) 2245–2252.
[7] H. Kim, R.P. Camata, Y.K. Vohra, W.R. Lacefield, Control of phase composition in hydroxyapatite/tetracalcium phosphate biphasic thin coatings for biomedical implants, J. Mater. Sci.: Mater. Med. 16 (2005) 961–966.
[8] K. Kazuhiko, S. Hironobu, Y. Tamoyuki, Local environment analysis of Mn ions in beta-tricalcium phosphate, J. Jpn. Ceram. Soc. 116 (2008) 108–110.
[9] I. Mayer, F.J.G. Cuisinier, I. Popov, Y. Schleich, S. Gdalya, O. Burghaus, D. Reinen, Phase relation between β-tricalcium phosphate and hydroxyapatite with manganese (II): structural and spectroscopic properties, Eur. J. Inorg. Chem. 2006 (2006) 1460–1465.
[10] W. Acchar, E.G. Ramalho, Effect of MnO_2 addition on sintering behavior of tricalcium phosphate: preliminary results, Mater. Sci. Eng. C 28 (2008) 248–252.
[11] I. Mayer, F.J.G. Cuisinier, S. Gdalya, I. Popov, TEM study of the morphology of Mn^{2+}-doped calcium hydroxyapatite and β-tricalcium phosphate, J. Inorg. Biochem. 102 (2008) 311–317.
[12] C. Reilly, The Nutritional Trace Metals, Blackwell, Oxford, 2004.
[13] I. Mayer, H. Diab, D. Reinen, Ch. Albercht, Manganese in apatites, chemical, ligand-field and electron paramagnetic resonance spectroscopy studies, J. Mater. Sci. 28 (1993) 2428–2432.
[14] I. Sopyan, A.N. Natasha, Preparation of nanostructured manganese-doped biphasic calcium phosphate powders via sol–gel method, Ionics 15 (2009) 735–741.
[15] Y. Masuda, K. Matsubara, S. Sakka, Synthesis of hydroxyapatite from metal alkoxides through sol–gel technique, Nippon Seramikkusu Kyokai Gakujitsu Ronbunshi 98 (1990) 1255–1266 (in Japanese).
[16] Y. Li, C.P.A.T. Klein, X. Zhang, K. de Groot, Relationship between the colour change of hydroxyapatite and the trace element manganese, Biomaterials 14 (1993) 969–972.
[17] S. Kannan, J.M.G. Ventura, J.M.F. Ferreira, Synthesis and thermal stability of potassium substituted hydroxyapatites and hydroxyapatite/β-tricalcium phosphate mixtures, Ceram. Int. 33 (2007) 1489–1494.
[18] H.S. Ryu, K.S. Hong, J.K. Lee, D.J. Kim, Variations of structure and composition in magnesium incorporated hydroxyapatite/β-calcium phosphate, J. Mater. Res. 21 (2006) 428–436.
[19] A. Jillavenkatesa, R.A. Condrate, Sol–gel processing of hydroxyapatite, J. Mater. Sci. 33 (1998) 4111–4119.
[20] A. Rapacz-Kmita, C. Paluszkiewicz, A. Slosarczyk, Z. Paszkiewicz, FTIR and XRD investigations on the thermal stability of hydroxyapatite during hot pressing and pressureless sintering processes, J. Mol. Struct. 744–747 (2005) 653–656.
[21] R. Morrissey, L.M. Rodriguez-Lorenzo, K.A. Gross, Influence of ferrous iron incorporation on the structure of hydroxyapatite, J. Mater. Sci.: Mater. Med. 16 (2005) 387–392.
[22] S. Lazic, S. Zec, N. Miljevic, S. Milonjic, The effect of temperature on the properties of hydroxyapatite precipitated from calcium hydroxide and phosphoric acid, Thermochim. Acta 374 (2001) 13–22.
[23] C.Y. Ooi, M. Hamdi, S. Ramesh, Properties of hydroxyapatite produced by annealing of bovine bone, Ceram. Int. 33 (2007) 1171–1177.
[24] A. Milev, G.S.K. Kannangara, B. Ben-Nissan, Morphological stability of hydroxyapatite precursor, Mater. Lett. 57 (2003) 1960–1965.
[25] E. Landi, G. Logroscino, L. Proietti, A. Tampieri, M. Sandri, S. Sprio, Biomemitic Mg-substituted hydroxyapatite: from synthesis to in vivo behaviour, J. Mater. Sci.: Mater. Med. 19 (2008) 239–247.
[26] Y.M. Kong, H.E. Kim, H.W. Kim, Phase conversion of tricalcium phosphate into Ca-deficient apatite during sintering of hydroxyapatite–tricalcium phosphate biphasic ceramics, J. Biomed. Mater. Res. B 84 (2007) 334–339.
[27] O. Prokopiev, I. Sevostianov, Dependence of the mechanical properties of sintered hydroxyapatite on the sintering temperature, Mater. Sci. Eng. A 431 (2006) 218–227.

[28] N.Y. Mostafa, Characterization, thermal stability and sintering of hydroxyapatite powders prepared by different route, Mater. Chem. Phys. 94 (2005) 333–341.
[29] H.R. Ramay, M. Zhang, Preparation of porous hydroxyapatite scaffolds by combination of the gel-casting and polymer sponge methods, Biomaterials 24 (2003) 3293–3302.
[30] E. Landi, A. Tampieri, G. Celotti, S. Sprio, Densification behaviour and mechanisms of synthetic hydroxyapatites, J. Eur. Ceram. Soc. 20 (2000) 2377–2387.
[31] J. Li, H. Liao, L. Hermansson, Sintering of partially-stabilized zirconia and partially-stabilized zirconia–hydroxyapatite composites by hot isostatic pressing and pressureless sintering, Biomaterials 17 (1996) 1787–1790.
[32] J.L. Xu, K.A. Khor, R. Kumar, Physicochemical differences after densifying radio frequency plasma sprayed hydroxyapatite powders using spark plasma and conventional sintering techniques, Mater. Sci. Eng. A 457 (2007) 24–32.
[33] I.R. Gibson, S. Ke, S.M. Best, W. Bonfield, Effect of powder characteristics on the sinterability of hydroxyapatite powders, J. Mater. Sci.: Mater. Med. 12 (2001) 1163–1171.
[34] H.A. Bhatt, S.J. Kalita, Influence of oxide-based sintering additives on densification and mechanical behavior of tricalcium phosphate (TCP), J. Mater. Sci.: Mater. Med. 18 (2007) 883–893.
[35] G. Muralithran, S. Ramesh, The effects of sintering temperature on the properties of hydroxyapatite, Ceram. Int. 26 (2000) 221–230.